Quantitative Micro-Elastography Enables *In Vivo* Detection of Residual Cancer in the Surgical Cavity during Breast-Conserving Surgery

Peijun Gong[1,2], Synn Lynn Chin[3], Wes M. Allen[1,2], Helen Ballal[3], James D. Anstie[1,2], Lixin Chin[1,2], Hina M. Ismail[1,2], Renate Zilkens[1,4], Devina D. Lakhiani[1,2], Matthew McCarthy[5], Qi Fang[1,2], Daniel Firth[1,2], Kyle Newman[1,2], Caleb Thomas[1,2], Jiayue Li[1,2,6], Rowan W. Sanderson[1,2], Ken Y. Foo[1,2], Chris Yeomans[7], Benjamin F. Dessauvagie[7,8], Bruce Latham[7,9], Christobel M. Saunders[3,4,10], and Brendan F. Kennedy[1,2,6]

ABSTRACT

Breast-conserving surgery (BCS) is commonly used for the treatment of early-stage breast cancer. Following BCS, approximately 20% to 30% of patients require reexcision because postoperative histopathology identifies cancer in the surgical margins of the excised specimen. Quantitative micro-elastography (QME) is an imaging technique that maps microscale tissue stiffness and has demonstrated a high diagnostic accuracy (96%) in detecting cancer in specimens excised during surgery. However, current QME methods, in common with most proposed intraoperative solutions, cannot image cancer directly in the patient, making their translation to clinical use challenging. In this proof-of-concept study, we aimed to determine whether a handheld QME probe, designed to interrogate the surgical cavity, can detect residual cancer directly in the breast cavity *in vivo* during BCS. In a first-in-human study, 21 BCS patients were scanned *in vivo* with the QME probe by five surgeons. For validation, protocols were developed to coregister *in vivo* QME with postoperative histopathology of the resected tissue to assess the capability of QME to identify residual cancer. In four cavity aspects presenting cancer and 21 cavity aspects presenting benign tissue, QME detected elevated stiffness in all four cancer cases, in contrast to low stiffness observed in 19 of the 21 benign cases. The results indicate that *in vivo* QME can identify residual cancer by directly imaging the surgical cavity, potentially providing a reliable intraoperative solution that can enable more complete cancer excision during BCS.

Significance: Optical imaging of microscale tissue stiffness enables the detection of residual breast cancer directly in the surgical cavity during breast-conserving surgery, which could potentially contribute to more complete cancer excision.

Introduction

Breast-conserving surgery (BCS) is the most common procedure for the treatment of early-stage breast cancer in many jurisdictions, including the United States and Europe (1–3). Currently, ∼20% to 30% of BCS patients undergo reexcision because postoperative histopathology of the resected specimen identifies cancer in the margins (4, 5). Additionally, substantial variation in reexcision rates between physicians and institutions has been reported, with a recent study reporting that the physician level reexcision rate ranges from 0% to 91.7%, with more than 17.5% of the physicians having a reexcision rate greater than the expert consensus cutoff of 30% (6). These additional operations can produce substantial physical, psychological, and financial burdens for patients and can delay recommended adjuvant therapies (4, 7–9).

A number of intraoperative margin assessment methods have been developed to address the high reexcision rate, including variants of traditional pathology methods, in particular, frozen section analysis and imprint cytology, and emerging imaging methods based on spectroscopy, microscopy, tomography, and fluorescence (10–12). None of these methods have achieved broad clinical acceptance, largely because they have not been able to meet the requirements of both high diagnostic accuracy and practical implementation (10, 11, 13–17). More importantly, most techniques assess the margins of excised specimens, providing only an indirect indication of residual cancer in the cavity, making it challenging to relate cancer identified in a specimen to its corresponding location in the cavity. This often results in the surgeon resecting large regions of noncancerous tissue to avoid leaving residual cancer in the cavity (18, 19). Direct, *in vivo* assessment of residual cancer in the surgical cavity may provide a more accurate and practical solution that fits efficiently within the existing surgical workflow (14).

Quantitative micro-elastography (QME) is an optical imaging technique that visualizes microscale stiffness in three dimensions (3D) to depths of ∼1 mm in breast tissue (20). QME is based on optical coherence tomography (OCT; spatial resolution: ∼2–10 μm), which forms images based on optical backscattering from boundaries

[1]BRITElab, Harry Perkins Institute of Medical Research, QEII Medical Centre, Nedlands and Centre for Medical Research, The University of Western Australia, Perth, Western Australia, Australia. [2]Department of Electrical, Electronic and Computer Engineering, School of Engineering, The University of Western Australia, Perth, Western Australia, Australia. [3]Breast Centre, Fiona Stanley Hospital, Murdoch, Western Australia, Australia. [4]Division of Surgery, Medical School, The University of Western Australia, Perth, Western Australia, Australia. [5]OncoRes Medical, Perth, Western Australia, Australia. [6]Australian Research Council Centre for Personalised Therapeutics Technologies, Melbourne, Victoria, Australia. [7]PathWest, Fiona Stanley Hospital, Murdoch, Western Australia, Australia. [8]Division of Pathology and Laboratory Medicine, Medical School, The University of Western Australia, Perth, Western Australia, Australia. [9]The University of Notre Dame, Fremantle, Western Australia, Australia. [10]Breast Clinic, Royal Perth Hospital, Perth, Western Australia, Australia.

Corresponding Author: Peijun Gong, BRITElab, Harry Perkins Institute of Medical Research, Perth 6009, Australia. Phone: 61-8-6488-6774; E-mail: peijun.gong@uwa.edu.au

Cancer Res 2022;82:4093–104

doi: 10.1158/0008-5472.CAN-22-0578

within tissue and can be considered as an optical equivalent of ultrasound (21, 22). OCT is effective for the identification of adipose tissue, because of the distinctively low optical backscattering from within adipose cells, in contrast to other dense tissues including cancer and benign stroma, which both exhibit relatively high optical backscattering. As a solution to address OCT's limited ability to distinguish between cancer and the surrounding benign stroma (23–25), QME uses OCT to further image the microscale deformation introduced to tissue by a mechanical load (26). Image processing is used to convert measured deformation into microscale maps of tissue stiffness, determined from the ratio of microscale stress (force per unit area) at the tissue surface to corresponding microscale strain (local deformation) in the tissue (20). QME can identify breast cancer based on its elevated microscale stiffness (27, 28). A recent *ex vivo* QME study of BCS clinical specimens, performed on 90 patients, demonstrated a sensitivity and specificity of 92.9% and 96.4% (25), respectively, in the detection of cancer within 1 mm of the surface of wide local excision (WLE) specimens. However, existing QME techniques have been implemented using benchtop imaging systems and therefore cannot be performed *in vivo*, precluding imaging of the surgical cavity.

We hypothesized that the extension of QME to a handheld probe, specifically designed to interrogate the surgical cavity, can enable surgeons to identify residual cancer in the surgical cavity. The primary outcome, consistent with previous QME studies on excised specimens (25), is the correspondence of high microscale stiffness with regions of cancer. Secondary outcomes are the development of a protocol to coregister *in vivo* cavity scans with histopathology performed on resected tissue, and preliminary validation of the practicality of *in vivo* QME. Here, we demonstrate the initial proof of concept of *in vivo* QME for in-cavity identification of residual cancer during BCS based on its elevated microscale stiffness.

Materials and Methods

Study design

A first-in-human clinical study was performed in Fiona Stanley Hospital, Western Australia, with ethics approval from the South Metropolitan Health Service Human Research Ethics Committee (PRN: RGS0000000499) and registration with the Australian New Zealand Clinical Trials Registry (ANZCTR; ACTRN12619001157167) and Australian Therapeutic Goods Administration (TGA; Clinical Trial CT-2018-CTN-04145-1 v1 TGA CTN). This study was conducted in compliance with the tenets of the Declaration of Helsinki and National Statement on Ethical Conduct in Human Research (2007) in Australia. Only female candidates (age: ≥18 years) with histologically confirmed invasive or *in situ* carcinoma and who were candidates for BCS based on clinical and radiological evaluation were recruited. Patients who were pregnant, lactating, or unable to give consent were excluded. A total of 26 BCS patients were enrolled with written informed consent received from all patients prior to the surgery. Twenty-one patients (19 patients undergoing initial WLE surgery and 2 patients undergoing reexcision surgery) were scanned with *in vivo* QME. The two reexcision patients were included to provide a more comprehensive assessment of *in vivo* QME. Five patients were consented but not scanned due to changes in the surgery schedule.

Clinical workflow

Prior to clinical scanning, the electrical and biological safety of the QME probe was confirmed at the hospital. Each surgeon was trained to use the QME probe on breast-mimicking phantoms (29), minimizing the risk of misusing the QME probe. Each surgeon reported that the probe was straightforward and comfortable to use after a single, 1-hour training session. Importantly, no significant variations in the QME image quality were observed between surgeons. The QME probe was then sterilized using hydrogen peroxide (STERRAD 100NX, Advanced Sterilization Products). At the beginning of the surgery, the surgeon prepared the probe for imaging in the sterile field. The surgeon placed a sterilized compliant silicone layer on the probe tip to enable measurement of the force exerted on the cavity tissue and applied sterile ultrasound gel and saline for lubrication (20). As an extra barrier to minimize the potential risk of infection, the probe was then placed in a sterile sheath (5-70340 KIT, Sheathing Technologies Inc.).

In vivo QME was integrated with the standard surgical workflow using the clinical protocol illustrated in **Fig. 1**. For the 19 WLE patients, the surgeon first resected the WLE specimen (Step 1) and placed it in the intraoperative specimen radiography (IOSR) device (Trident, Hologic Inc.) for assessment (Step 2). From analysis of the margins in the IOSR image and, also, from palpation, the surgeon decided if, and from which cavity aspects, a cavity shaving would be taken at Step 4. A cavity aspect is the location in the surgical cavity corresponding to the anatomic orientation of the breast, as defined in Supplementary Table S1 and illustrated in Supplementary Fig. S1 (30). A cavity shaving, as defined in Supplementary Table S1, is the additional tissue removed after resection of the main WLE specimen if the surgeon suspects that residual cancer remains in the cavity (31, 32). Prior to taking cavity shavings, the surgeon placed the QME probe in the cavity to scan the aspects where cavity shavings would subsequently be taken (Step 3). If the surgeon decided not to take a cavity shaving, he/she scanned selected cavity aspects of interest. Importantly, the decision to take a cavity shaving followed current standard-of-care protocols and was not influenced by QME images. To ensure this, the surgeon made the decision on taking a cavity shaving prior to scanning and was also blinded to the QME cancer evaluation (i.e., QME-determined cancer presence/absence) during the surgery.

For the two reexcision patients, the surgeon reopened the surgical site and scanned the cavity aspects for reexcision, as determined by histopathology of the resected specimen from the previous BCS surgery. For simplicity, the subsequently excised tissue is also referred to as a cavity shaving.

During *in vivo* QME scanning, the surgeon first briefly surveyed the selected cavity aspect using the real-time imaging capability of the probe and identified regions of mainly dense tissue (i.e., regions not dominated by adipose tissue). Subsequently, 3D scans of a tissue volume of $6 \times 6 \times 3.6$ mm ($364 \times 364 \times 1{,}024$ pixels) were acquired. The acquisition time for each 3D scan was 3.3 seconds. To provide support and to ensure that adequate force was applied to the region scanned by the probe, the surgeon typically used the non-probe hand to provide back support to the breast.

After QME scanning, the surgeon completed the procedure following standard protocols used in the hospital. The WLE specimen and cavity shavings (if taken) were immediately transferred to an adjacent laboratory for routine postoperative histopathology and coregistration with *in vivo* QME (Step 5 in **Fig. 1**). As shown in **Fig. 1**, the regions of the cavity scanned with *in vivo* QME corresponded directly to the tissue removed as a cavity shaving and were adjacent to the WLE specimen. Thus, histopathology of the cavity shaving provided a more direct validation of *in vivo* QME. However, a cavity shaving was taken only if deemed necessary by the surgeon for the treatment of the patient. Subsequently, in some instances (23 scanned cavity aspects) as shown in Step 5 in **Fig. 1**, histopathology performed on the cavity

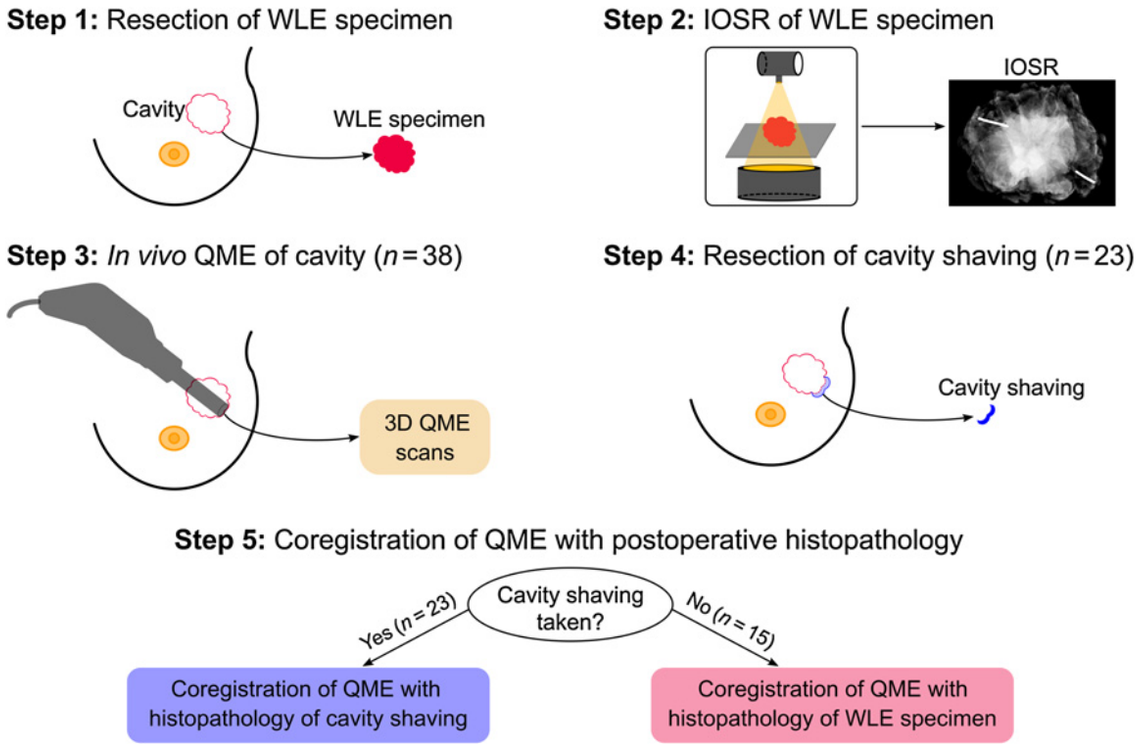

Figure 1.
Illustration of the clinical protocol used in the study.

shavings was coregistered with *in vivo* QME acquired prior to the cavity shaving being taken. In the other 15 scanned cavity aspects, QME was coregistered with histopathology of the WLE specimen in the region adjacent to that scanned in the cavity using QME.

QME scanning

The QME system comprises an OCT imaging stack and a handheld probe unit. It provides an axial and lateral OCT resolution of 5.5 μm (in air) and 14.1 μm, respectively, at a center wavelength of 1,300 nm and an axial line scan (A-scan) rate of 146 kHz. The handheld probe incorporates an optical subsystem for OCT imaging and a mechanical subsystem (an annular piezoelectric actuator) to impart compressive loading to the tissue (20, 28). The OCT subsystem uses spectral-domain OCT and operates in a common-path configuration (33). A video camera is also embedded in the probe to photograph the tissue being imaged by QME, facilitating coregistration with postoperative histopathology.

To avoid imaging artifacts caused by the motion of the patient or surgeon, the microelectromechanical systems (MEMS) scanning mirror incorporated in the probe enabled cross-sectional OCT images (B-scans) to be acquired at 220 Hz, providing a 3D scan acquisition time of 3.3 seconds. The annular piezoelectric actuator was synchronized with the optical scanning, allowing the tissue to be deformed up to 20 μm between OCT B-scan acquisitions. At each lateral location, a pair of OCT B-scans were acquired, one before and one after mechanical loading, from which the stiffness at each pixel was determined in real time using image processing algorithms with graphics processing unit acceleration (20). Briefly, the signal processing used OCT B-scan pairs to estimate the axial microstrain resulting from mechanical loading at each location within the OCT volume. By relating this microstrain to the corresponding stress at the tissue surface measured by the compliant silicone layer, the spatially resolved, microscale stiffness of the tissue is presented in QME images (see Supplementary Note for more technical details on both OCT and QME; ref. 20).

Representative OCT/QME B-scans and *en face* images (i.e., images parallel to the tissue surface) from 3D scans acquired from four patients are shown in Results. OCT images are displayed in grayscale on a logarithmic scale from 0 to 29–35 dB. QME images are displayed in false color on a logarithmic scale from 1 to 500 kilopascals (kPa) and, for the *en face* images, are overlaid on the corresponding OCT images with local regions masked to show QME in dense tissue (25, 33).

QME cancer evaluation

En face images of tissue stiffness from 3D QME scans were subsequently used to determine the presence or absence of cancer in the scanned cavity tissue. QME cancer criteria established in a previous *ex vivo* diagnostic accuracy study were utilized in *in vivo* QME scans to determine the presence of cancer (25). Following these criteria, high stiffness was defined as >26 kPa (25). Cancer was considered present when the QME scan contained an area of high stiffness covering ≥75% of a 1-mm circle in the *en face* images (25).

Postoperative histopathology

All WLE specimens (Supplementary Fig. S2A) and cavity shavings were inked to mark corresponding aspects of the cavity and were cut in a bread loafing manner into multiple ∼4- to 5-mm-thick sections (Supplementary Fig. S2B). If the dimension of the section was too large to fit onto a single histopathology slide, the section was further divided

into multiple blocks (Supplementary Fig. S2C). These sections/blocks were fixed in formalin, processed, embedded in paraffin, cut into histopathology slices, and stained with hematoxylin and eosin, with one histopathology slide imaged from each section/block (Supplementary Fig. S2D) and subsequently annotated by experienced pathologists (Fellows of the Royal College of Pathologists of Australasia). This created an image series with a spacing of ∼4 to 5 mm, with a similar slide orientation to that of the OCT B-scans acquired with the probe in the cavity. WLE margins adjacent to the cavity tissue scanned with QME and cavity shaving margins from the cavity side scanned with QME before the cavity shaving was taken were classified as positive (cancer at the tissue surface), close (no cancer at the tissue surface but cancer within ∼1 mm of the tissue surface) or negative (no cancer within ∼1 mm of the tissue surface; refs. 25, 34–36), following the protocol established in the previous *ex vivo* diagnostic accuracy study (25).

Image coregistration

B-scans in the 3D OCT scans acquired with the probe were manually coregistered with a series of histopathology images similar to those shown in Supplementary Fig. S2D and S2E (33). For scans where a cavity shaving was taken, this process involved matching distinctive features in OCT images, such as the morphology of adipose tissue and dense tissue with corresponding features in histopathology images. For scans where cavity shavings were not taken, similar correspondence was identified between OCT B-scans and the WLE histopathology corresponding to the tissue adjacent to that scanned with QME in the cavity. Coregistration was achieved for all 38 scanned cavity aspects, including the 23 cases with available cavity shavings and the 15 cases with only WLE specimens (Step 5 in **Fig. 1**). However, close and negative margins from the WLE specimens (13 of the 15 cases) were not used for validation of *in vivo* QME because they could not adequately confirm the presence or absence of cancer to 1 mm depth in *in vivo* QME scans of the cavity, as described in Results.

Data availability

The data generated in this study are available within the article and Supplementary Table S2. The raw OCT and QME data generated in this study are available upon request from the corresponding author.

Results

QME results summary

In vivo QME was performed on 38 cavity aspects from 21 patients by five surgeons (1.8 ± 0.5 cavity aspects scanned per patient) undergoing initial BCS surgery ($n = 19$) or reexcision ($n = 2$; Supplementary Table S2). WLE specimens from all 19 WLE patients underwent IOSR. Cavity shavings were taken at a rate of 1.1 ± 0.7 cavity shavings per patient. **Table 1** summarizes the clinical characteristics of the 21 BCS patients.

As illustrated in **Fig. 2**, coregistered histopathology of the WLE specimens and cavity shavings identified cancer in four cavity aspects scanned from four patients, based on one positive and one close margin in the cavity shavings, and two positive margins in the WLE specimens. Coregistered histopathology of the cavity shavings identified no residual cancer for 21 scanned cavity aspects based on negative cavity shaving margins. For the remaining 13 scanned cavity aspects, coregistered histopathology showed close ($n = 1$) or negative ($n = 12$) WLE margins with no available cavity shavings, which could not sufficiently indicate the cancer presence/absence in the scanned cavity aspects.

Table 1. Clinical characteristics of the 21 BCS patients.

	***N* (%) or mean ± SD**
Age (y)	54.6 ± 11.2
BMI (kg/m^2)	27.8 ± 7.7
Neoadjuvant treatment	2 (9.5)
WLE procedure	
Hookwire	1 (4.8)
Iodine-125 seed	13 (61.9)
Intraoperative specimen radiography	19 (90.5)
Duration of surgery (minutes)	61.4 ± 23.2
Number of cavity shavings per patient	1.1 ± 0.7
WLE pathology[a]	
Invasive malignancy[b]	13 (61.9)
DCIS	10 (47.6)
Pleomorphic LCIS	1 (4.8)
Cavity shaving pathology[a]	
Invasive malignancy	1 (4.8)
DCIS	2 (9.5)
LCIS	2 (9.5)

Abbreviations: BMI, body mass index; LCIS, lobular carcinoma *in situ*.
[a]Pathology includes all cancers both within and beyond 1 mm of all margins.
[b]Invasive malignancy comprised 11 invasive ductal carcinomas not otherwise specified, one mixed, and one with colloid (mucinous) ductal not otherwise specified and mixed.

In all four cancer cases confirmed by coregistered histopathology, QME presented elevated microscale stiffness indicative of cancer based on the cancer criteria published previously (25). All four patients received follow-up reexcision surgery. In contrast, QME of 19 of 21 scanned cavity aspects with negative cavity shaving margins presented low stiffness. In total, *in vivo* QME of 25 scanned cavity aspects was validated using the coregistered histopathology of the WLE specimens or cavity shavings, as shown in **Fig. 2**. For the remaining 13 cavity aspects, QME was coregistered with histopathology of the WLE margins (i.e., no available cavity shavings), but conclusive validation was not possible, as the close ($n = 1$) or negative ($n = 12$) WLE margins were considered ambiguous predictors of the presence or absence of cancer in the surgical cavity. Details and QME results of all these scanned cavity aspects are summarized in Supplementary Table S2. Below, representative images are presented that demonstrate the capability of QME to identify cancer, based on high stiffness (**Figs. 3** and **4**), and benign tissue, based on low stiffness (**Figs. 5** and **6**).

QME of ductal carcinoma *in situ*

Results from Cavity Aspect 1 of Patient 2 [age: 56 years, body mass index (BMI): 33.3 kg/m^2] in Supplementary Table S2 are presented in **Fig. 3**, including the *en face* OCT and QME images, respectively, in **Fig. 3A** and **B**, OCT and QME B-scans, respectively, in **Fig. 3C** and **D**, coregistered histopathology in **Fig. 3E** and IOSR image in **Fig. 3F**. An iodine-125 seed was used to guide the resection of the impalpable cancer in the left breast of the patient (37). During surgery, IOSR of the WLE specimen (**Fig. 3F**) did not indicate cancer in the margins, which contributed to the decision of no additional cavity shaving. However, postoperative histopathology identified multiple regions of ductal carcinoma *in situ* (DCIS; arrowheads in **Fig. 3E**) at the lateral margin of the WLE specimen. Consequently, the patient had a follow-up reexcision surgery ∼12 weeks after the initial BCS surgery.

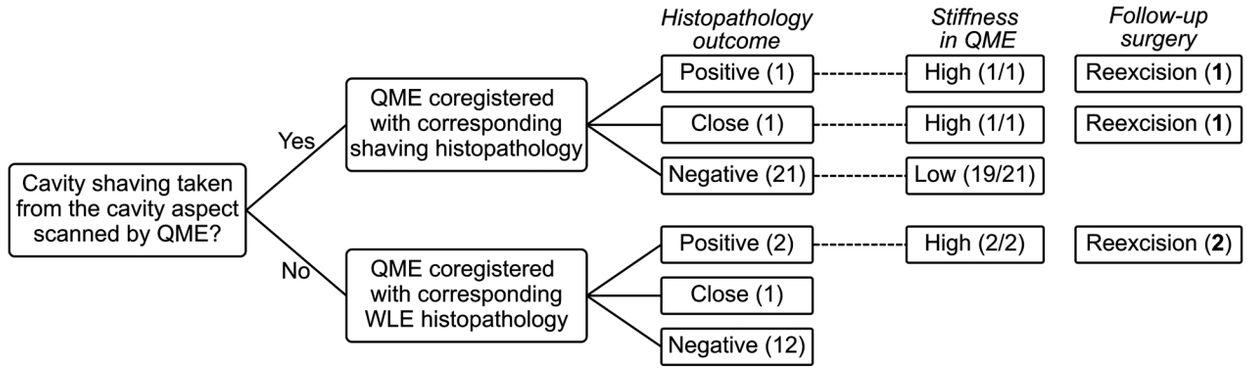

Figure 2.

Classification of the 38 cavity aspects from 21 BCS patients scanned with *in vivo* QME. The numbers in the right three columns indicate the number of scanned cavity aspects in each scenario, the ratio of the scanned cavity aspects showing high or low stiffness in QME, and the number of patients who underwent follow-up reexcision surgery corresponding to high stiffness, respectively. When QME of the cavity tissue is coregistered with the cavity shaving histopathology, as listed in Supplementary Table S2, the positive ($n = 1$) and close ($n = 1$) margins indicate the presence of cancer in the scanned cavity aspects and thus the expected high stiffness in QME, whereas the negative margins ($n = 21$) indicate the absence of cancer in the scanned cavity aspects and thus the expected low stiffness in QME. When QME is coregistered with histopathology of the WLE margin adjacent to the cavity tissue scanned by QME, only positive margins ($n = 2$) can indicate the presence of cancer in the scanned cavity aspects and thus expected high stiffness in QME, whereas close ($n = 1$) and negative ($n = 12$) margins are ambiguous predictors of the presence or absence of cancer in the surgical cavity and thus cannot be used to validate QME.

QME scanning was performed on the lateral aspect of the surgical cavity, with the *en face* OCT and QME images shown in **Fig. 3A** and **B**, where the tissue presents local regions of elevated stiffness in **Fig. 3B**. **Figure 3C–E** presents coregistration of the OCT/QME B-scans with histopathology. The scanned cavity tissue is adjacent to the WLE specimen of the same lateral aspect and presents a similar tissue structure at the surface (left to right: cancer/stroma/adipose tissue). The identified cancer in **Fig. 3E** presents the common characteristics of DCIS: clonal proliferation of malignant-appearing cells within the lumens of the mammary ducts. The DCIS at the WLE specimen surface (top arrowhead; with a possible tearing from the stroma to its right) is confined to a local region and corresponds to the moderately low OCT signal in **Fig. 3C** but, consistent with previous *ex vivo* QME studies, it is difficult to differentiate DCIS based solely on the OCT signal (25). In contrast, the corresponding QME B-scan in **Fig. 3D** clearly identifies the region of DCIS as a local region of elevated stiffness in the cavity.

In the *en face* QME image in **Fig. 3B**, taken from a depth of 100 μm below the tissue surface, the elevated stiffness reaches ∼300 to 400 kPa, with an area of high stiffness larger than a 1-mm circle. Using the QME criteria for cancer (25), we determined that this region corresponded to cancer present in the lateral aspect of the cavity, consistent with the positive margin in the WLE specimen identified by histopathology that was coregistered with the OCT/QME images in **Fig. 3**.

QME of invasive ductal carcinoma

Results from Cavity Aspect 2 of Patient 16 (age: 47 years, BMI: 22.1 kg/m^2) are presented in **Fig. 4**. The *en face* OCT and QME images, OCT and QME B-scans, coregistered histopathology, and IOSR image are shown, respectively, in **Fig. 4A–F**. This patient received WLE of the right breast without hookwire or iodine-125 seeds. IOSR during surgery indicated possible cancer with high intensity at the medial to superior-medial margin (**Fig. 4F**), contributing to the decision to take a cavity shaving from the superior-medial aspect of the cavity and no cavity shaving from the lateral aspect of the cavity. Postoperative histopathology identifies invasive ductal carcinoma (IDC) at the lateral margin of the WLE specimen (**Fig. 4E**), corresponding to the lateral cavity aspect scanned by the QME probe. Consequently, the patient underwent a reexcision surgery ∼2 weeks after the initial BCS surgery.

OCT from the lateral aspect of the cavity in **Fig. 4A** and **C** shows mainly dense tissue with several structural features (e.g., horizontal strips of tissue in **Fig. 4C**), but it is difficult to determine what this dense tissue corresponds to. QME in **Fig. 4B** and **D** shows elevated stiffness scattered across the image with high values in the range of 70 to 400 kPa in regions extending over several millimeters, indicating the presence of cancer in the lateral aspect of the cavity, consistent with IDC reported by histopathology (**Fig. 4E**). In addition, the surgeon scanned the superior-medial aspect of the cavity with the probe (Cavity Aspect 21 in Supplementary Table S2) before taking the cavity shaving. QME images show markedly lower stiffness in this region, below the threshold for cancer, which is consistent with the absence of cancer in the cavity shaving assessed by postoperative histopathology.

QME of benign tissue

In contrast to the observed high stiffness of cancer, benign tissue is characterized by markedly lower stiffness in QME (25). Representative cases of benign cavity aspects are presented in **Figs. 5** and **6**, respectively. The *en face* OCT and QME images, OCT and QME B-scans, coregistered histopathology, and IOSR image from Patient 3 (age: 45 years, BMI: 21.2 kg/m^2), are shown, respectively, in **Fig. 5A–F**. Based on IOSR of the WLE specimen presented in **Fig. 5F**, the surgeon decided to take cavity shavings from the superior-lateral and the superior-medial cavity, respectively, due to the observed calcification (marked C in **Fig. 5F**). Prior to resecting the cavity shaving, QME was performed on both cavity aspects with the results from the superior-lateral aspect of the cavity (Cavity Aspect 7) shown in **Fig. 5**. Postoperative histopathology identifies close margins in the WLE specimen corresponding to these cavity aspects, and the absence of cancer in the two cavity shavings.

QME (**Fig. 5B** and **D**) shows predominantly low stiffness (<10 kPa), although there is a local region of moderate stiffness (red arrow). Using the QME cancer criteria, **Fig. 5B** indicates that there is no cancer in the scanned cavity tissue, which is consistent with the absence of cancer in

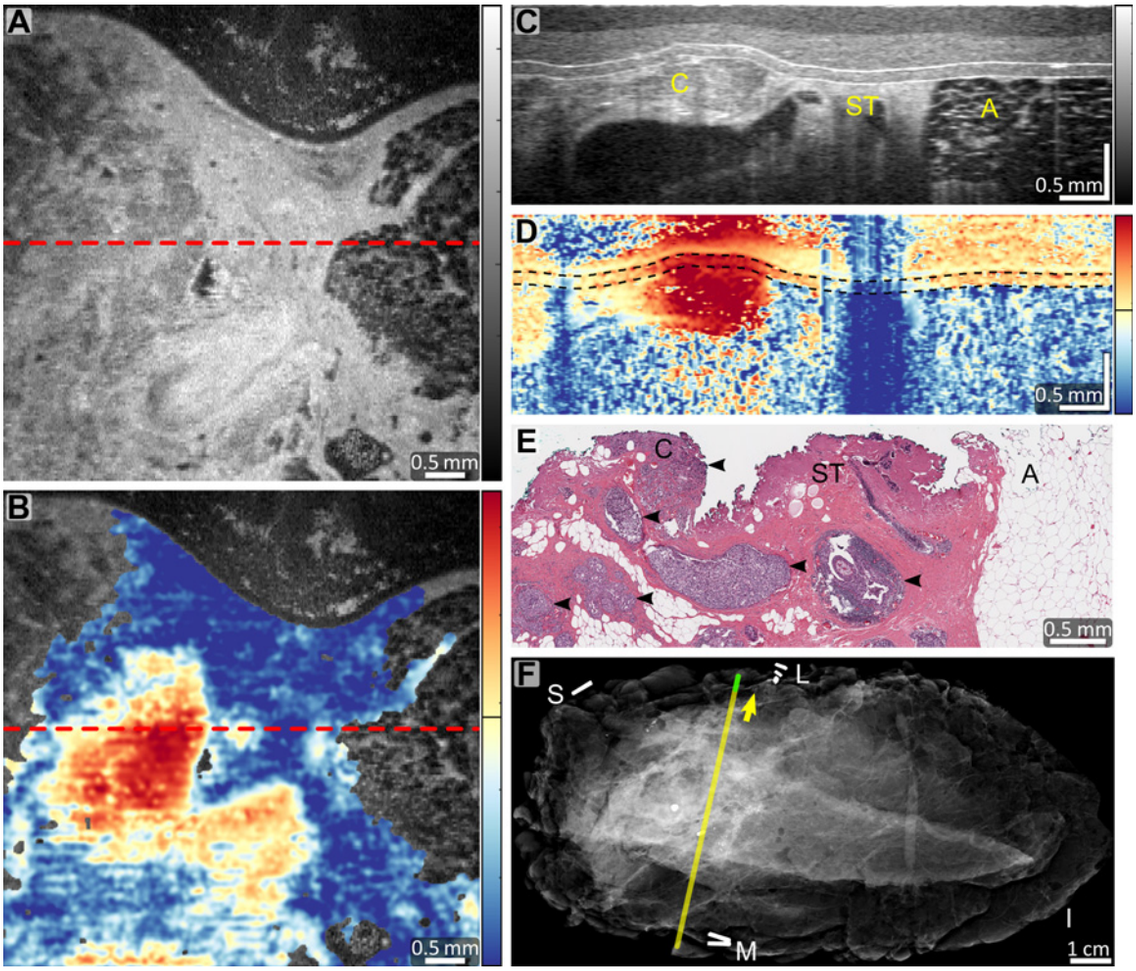

Figure 3.

Imaging of the lateral aspect of the surgical cavity of Patient 2. **A** and **B,** *En face* OCT (**A**) and *en face* QME (**B**) at a depth of 100 μm below the tissue surface. **C** and **D,** OCT B-scan (**C**) and QME B-scan (**D**) from the locations indicated by the dashed lines in **A** and **B**, respectively. Dashed lines in **D** mark the silicone layer-sheath and sheath-tissue interfaces. Color bars, OCT 0–33 dB; QME 1–500 kPa with the black line marking 26 kPa. **E,** Coregistered histopathology of the WLE specimen at the lateral margin. Arrowheads, regions of DCIS. **F,** IOSR of the WLE specimen. The yellow arrow marks the region adjacent to that imaged by QME in the cavity. The yellow line marks the approximate location of the histopathology slide matched to OCT and QME. **E** is extracted from a location at the green line in **F**. A, adipose tissue; C, cancer; ST, stroma; I, inferior; L, lateral; M, medial; S, superior.

the cavity shaving by postoperative histopathology, as shown in **Fig. 5E**.

Results from Patient 6 (age: 49 years, BMI: 24.8 kg/m^2) are presented in **Fig. 6**. The *en face* OCT and QME images, OCT and QME B-scans, coregistered histopathology, and IOSR image are shown respectively in **Fig. 6A–F**. Based on IOSR of the WLE specimen (**Fig. 6F**) and palpation, the surgeon took cavity shavings from the inferior and lateral aspects of the cavity. As the WLE specimen and two cavity shavings all showed negative margins in histopathology, the patient did not receive a follow-up surgery. Prior to taking the cavity shavings, *in vivo* QME was performed on both the inferior and lateral aspects of the cavity and showed low stiffness, indicating no cancer. QME and OCT of the inferior aspect of the cavity (Cavity Aspect 12) are shown in **Fig. 6A–D**, where an outlined region of high stiffness in **Fig. 6B** was created by a marking suture, as validated in Supplementary Fig. S3. In this validation, an additional scanning of the cavity shaving using a benchtop OCT scanner (Supplementary Fig. S3A–S3C) was performed, followed by coregistration of the photograph (Supplementary Fig. S3A) and OCT images (Supplementary Fig. S3B and S3C) to those from *in vivo* QME scanning of cavity (Supplementary Fig. S3D–S3H).

Discussion

This study presents the proof of concept of *in vivo* QME for direct imaging of the surgical cavity and the capability to identify residual cancer. The elevated microscale stiffness of cancer observed, including in DCIS and IDC, in contrast to the much lower stiffness of the benign tissue, demonstrates the potential for cancer detection. In addition, this study demonstrates the feasibility of integrating *in vivo* QME into the standard surgical workflow and a coregistration protocol to validate the *in vivo* results. Supported by the high sensitivity and specificity previously determined in an *ex vivo* QME study of WLE specimens (25), *in vivo* QME has the potential to contribute to a more complete removal of cancer while avoiding unnecessarily large cavity

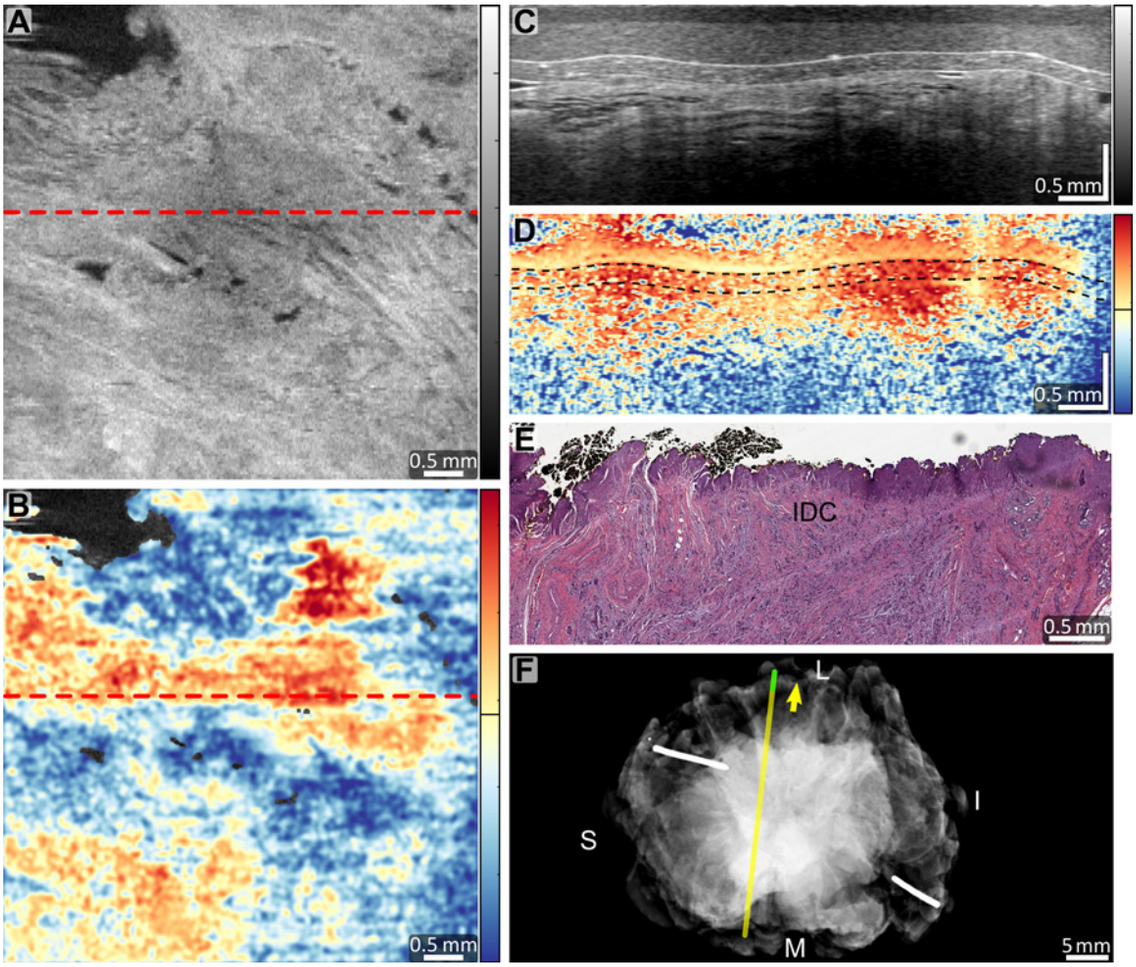

Figure 4.

Imaging of the lateral aspect of the surgical cavity of Patient 16. **A** and **B,** *En face* OCT (**A**) and *en face* QME (**B**) at a depth of 100 μm below the tissue surface. **C** and **D,** OCT B-scan (**C**) and QME B-scan (**D**) from the locations indicated by the dashed lines in **A** and **B**, respectively. Dashed lines in **D** mark the silicone layer–sheath and sheath–tissue interfaces. Color bars, OCT 0–35 dB; QME 1–500 kPa with the black line marking 26 kPa. **E,** Coregistered histopathology of the WLE specimen at the lateral margin. **F,** IOSR of the WLE specimen. The yellow arrow marks the region adjacent to that imaged by QME in the cavity. The yellow line marks the approximate location of the histopathology slide matched to OCT and QME. **E** is extracted from a location at the green line in **F**. I, inferior; L, lateral; M, medial; S, superior.

shavings. Now that the proof-of-concept and clinical protocols have been established in this study, future studies will focus on performing *in vivo* QME on a large patient cohort to determine the diagnostic accuracy of *in vivo* QME in the detection of residual cancer in the cavity and will also investigate the clinical efficacy of *in vivo* QME for reducing reexcision surgery.

In-cavity QME was validated through coregistration with either postoperative histopathology of cavity shavings ($n = 23$) or WLE specimens ($n = 2$). This validation was enabled by the development of a custom coregistration protocol. In this protocol, cavity tissue scanned by *in vivo* QME was in the uppermost region of the cavity shaving (if taken) and was adjacent to the corresponding margin of the WLE specimen. When the cavity shaving showed positive ($n = 1$) or close ($n = 1$) margins, or when the WLE specimen corresponding to the cavity aspect scanned showed positive margins ($n = 2$) based on histopathology, the scanned cavity aspect was expected to have residual cancer. In all four such cases, QME observed elevated stiffness indicative of the presence of cancer. In contrast, when the cavity shavings ($n = 21$) showed negative margins based on histopathology, the scanned cavity aspects were expected to have no cancer, which largely agreed with the low stiffness detected by QME (19 of 21 scanned cavity aspects). The two false-positive cases might be due to excessive pressure applied to the tissue, indicated by an abnormally large reduction in the thickness of the silicone layer, which could be avoided in the future through additional surgeon training.

In the two cases with positive WLE margins, the use of coregistered histopathology to indicate the presence of cancer in the cavity assumes that the resection of the WLE specimen cut through the cancerous region and that residual cancer remained in the patient at the cavity surface. This assumption is the basis for the standard clinical practice used to determine if there is residual cancer in the cavity and, consequently, if reexcision is required. The closely matched tissue structures at the surface between the *in vivo* QME images and histopathology (e.g., **Fig. 3C** and **D** vs. **Fig. 3E**) suggest that this is

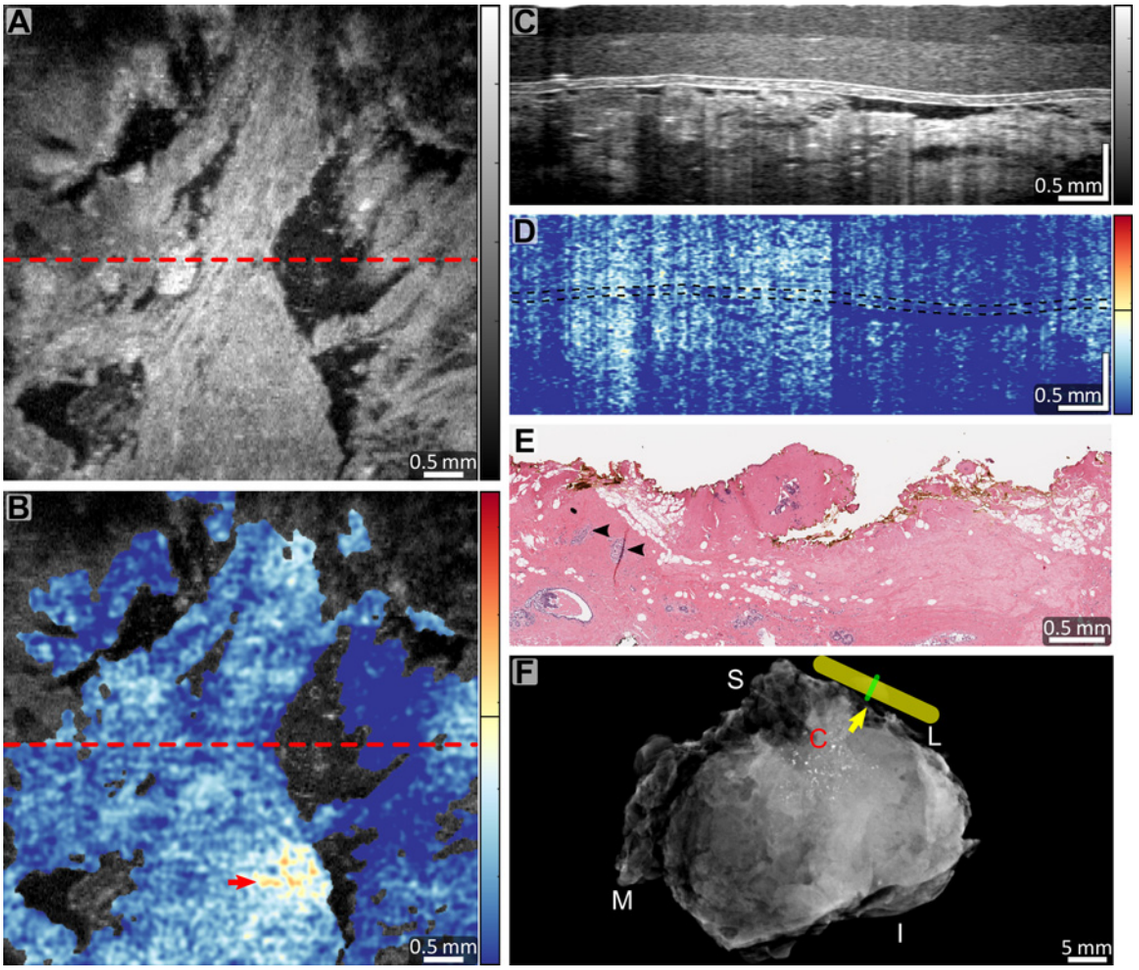

Figure 5.

Imaging of the superior-lateral aspect of the surgical cavity of Patient 3. **A** and **B,** *En face* OCT (**A**) and *en face* QME (**B**) at a depth of 100 μm below the tissue surface. Red arrow, local region of moderate stiffness. **C** and **D,** OCT B-scan (**C**) and QME B-scan (**D**) from the locations indicated by the dashed lines in **A** and **B**, respectively. Dashed lines in **D** mark the silicone layer-sheath and sheath-tissue interfaces. Color bars, OCT 0–30 dB; QME 1–500 kPa with the black line marking 26 kPa. **E,** Coregistered histopathology of the cavity shaving from the margin of the superior-lateral tissue. Arrowheads, local regions of benign terminal duct lobular units. **F,** IOSR of the WLE specimen. The yellow arrow marks the region adjacent to that imaged by QME in the cavity. The yellow bar marks the location where the superior-lateral cavity shaving was taken for histopathology. The green line indicates the slicing direction of the cavity shaving to generate the best match of histopathology (**E**) to OCT and QME. C, calcification; I, inferior; L, lateral; M, medial; S, superior.

an accurate validation method in the case of positive margins in the WLE specimen. To achieve a more complete validation of *in vivo* QME, in future studies, it would be preferable to modify the protocol such that *in vivo* QME is only performed on those cavity aspects with corresponding cavity shavings.

One limitation of the validation by histopathology is that a cavity shaving was not taken for some of the cavity aspects scanned ($n = 15$), determined by the surgeons based on IOSR and palpation. In these cases, close ($n = 1$) and negative ($n = 12$) margins in the WLE, determined by histopathology, were ambiguous predictors of the presence or absence of cancer in the scanned cavity aspects, as the WLE margins were adjacent to the cavity tissue scanned by QME. Consequently, a number of QME scans could not be validated, especially those corresponding to negative WLE margins ($n = 12$). Although current clinical practice is to consider that these cases indicate no cancer remaining in the cavity, we observed two cases (Cavity Aspects 3 and 4) with negative margins in the WLE that had positive or close margins in the corresponding cavity shavings, indicating cancer that would have remained in the cavity had the cavity shavings not been taken. Therefore, we did not use negative or close WLE margins without a cavity shaving to validate QME. Although these cases could not be validated, they largely presented low stiffness in *in vivo* QME images (12 of 13 as described in Supplementary Table S2), indicating the absence of cancer, which is consistent with an expected low risk of residual cancer using current clinical practice.

The study also included two reexcision patients to assess *in vivo* QME's capability to detect residual cancer, although they introduced heterogeneity to the study population, which mainly comprised patients undergoing initial BCS surgery. The purpose was to provide a more comprehensive assessment of *in vivo* QME as reexcision patients may also potentially benefit from *in vivo* QME by detecting residual cancer in the newly formed surgical cavity, thus reducing the

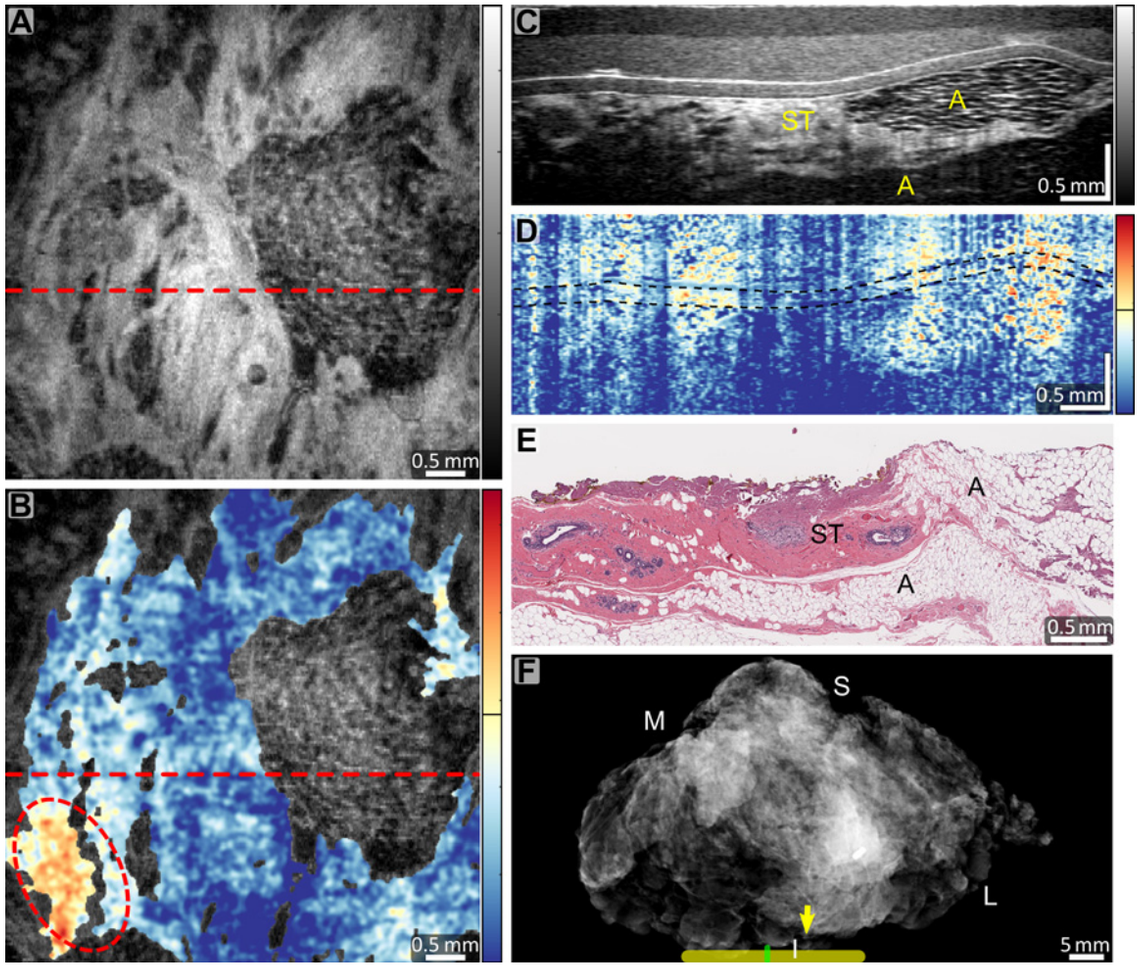

Figure 6.

Imaging of the inferior aspect of the surgical cavity of Patient 6. **A** and **B,** *En face* OCT (**A**) and *en face* QME (**B**) at a depth of 100 μm below the tissue surface. Outlined region in **B** shows an artifact due to a marking suture as identified in Supplementary Fig. S3. **C** and **D,** OCT B-scan (**C**) and QME B-scan (**D**) from the locations indicated by the dashed lines in **A** and **B**, respectively. Dashed lines in **D** mark the silicone layer–sheath and sheath–tissue interfaces. Color bars, OCT 0–29 dB; QME 1–500 kPa, with the black line marking 26 kPa. **E,** Coregistered histopathology of the cavity shaving from the margin of the inferior tissue. **F,** IOSR of the WLE specimen. The yellow arrow marks the region adjacent to that imaged by QME in the cavity. The yellow bar marks the location where the inferior cavity shaving was taken for histopathology. The green line indicates the slicing direction of the cavity shaving to generate the best match of histopathology (**E**) to OCT and QME. A, adipose tissue; ST, stroma; I, inferior; L, lateral; M, medial; S, superior.

chance of additional reexcision. However, to determine the diagnostic accuracy of *in vivo* QME in well-powered future studies, the heterogeneity of the study population will need to be carefully considered.

In vivo QME could potentially be used as an intraoperative adjunct to complement existing clinical procedures. In general, the goal of intraoperative imaging during BCS is to provide a more complete removal of cancer during surgery so that the pathologist observes fewer positive margins in the resected specimen, leading to a reduction in reexcision rates. However, it is not clear whether the reduced reexcision rate would affect the survival rate. Long-term follow-up studies on a large patient cohort in the future will be required to assess the impact (38, 39).

In the current scanning protocol, only selected local tissue regions inside the surgical cavity were scanned for preliminary validation, and the protocol was not designed to screen the entire surgical cavity. In the context of this proof-of-concept study, as *in vivo* QME was not used to inform patient treatment and standard postoperative histopathology was performed for routine assessment, failure to detect all residual cancer was not relevant. To avoid missing residual cancer in the cavity, and resulting false negatives, further development is needed to refine the protocol to allow all cavity aspects to be scanned after a more complete validation of *in vivo* QME. Such a protocol would allow us to determine the benefit of *in vivo* QME in providing more complete cancer detection and, potentially, in reducing the need for reexcision surgery.

On the macroscale, through palpation, utilizing the increased stiffness of breast cancer to identify cancer is an integral component of breast cancer surgery (40). Ultrasound elastography and magnetic resonance elastography have further demonstrated that breast cancer lesions can be identified based on elevated stiffness on the macroscale (41, 42). More recently, studies on the microscale have provided insight into the physiologic basis for this stiffening. These studies have

reported that breast tissue becomes progressively stiffer during tumorigenesis, and that this stiffening is often caused by increased collagen deposition and crosslinking, and extracellular matrix (ECM) deposition and remodeling (43–45). The metabolism of collagen, as the major scaffolding protein in ECM, is deregulated in cancer with increased collagen expression, elevated deposition, and altered organization (43), which contribute to increased stiffness. The increased stiffness also promotes the epithelial cell transformation toward cancer, promotes malignancy, and enhances cancer aggression (45, 46). Previous QME studies performed on *ex vivo* tissue have additionally demonstrated that densely packed cancer cells within the cancer microenvironment can manifest as elevated stiffness and that fluid pressure in mucinous carcinomas also presents as elevated stiffness (23, 25, 33). This finding has been further shown in Supplementary Fig. S4 (histopathology of four specimens in Supplementary Fig. S4A–S4D; corresponding *en face* OCT and QME images respectively in Supplementary Fig. S4E–S4H and Supplementary Fig. S4I–S4L) on *ex vivo* breast tissue including common cancer types of invasive lobular carcinoma (ILC), IDC, and DCIS.

In this study, hematoxylin and eosin staining was used for histopathology of the resected tissue to identify the tissue types for validating *in vivo* QME. Although other staining options, such as immunohistochemistry staining (47), could provide additional information, they have not been adopted to assess ECM constituents in the hospital where the study was performed, because of the lack of objective measures and challenges with reproducibility. Future studies could seek to use other alterative stains to further consolidate the physiologic basis of the elevated stiffness of breast cancer.

A variety of fluorescence-based methods have used cancer-specific proteins, antigens, enzymes, or pH to activate fluorescence for cancer detection with studies reporting excellent sensitivity (>90%) and accuracy (>90%; refs. 10, 48–50). Compared with fluorescence-based methods, *in vivo* QME uses endogenous mechanical contrast in tissue to provide label-free imaging, eliminating the need for the injection of exogenous contrast agents and the issue of the target enzymes or proteins not being expressed in all cancer types (10). The stiffness measured by *in vivo* QME does not vary over the time of the surgery, whereas some fluorescence methods provide a time-varying signal, complicating cancer detection and limiting the reproducibility of results and practical deployment (50). Additionally, *in vivo* QME provides 3D imaging to enable examination of the tissue microstructure and stiffness at different depths and locations of interest, in contrast to fluorescence images, which are generally two-dimensional. Yet, future studies are needed to assess which method will ultimately be most effective for intraoperative assessment during BCS. Another possibility is to combine imaging methods that use different contrast mechanisms into a multimodal approach, for example, based on both chemical and mechanical contrast, to enhance cancer detection.

A potential advantage of *in vivo* QME is that a quantitative tissue property is measured (i.e., microscale stiffness) to detect residual cancer in the cavity. The quantitative measurement enabled the adoption of the cancer criteria previously established in the accuracy study of *ex vivo* breast tissue to *in vivo* cavity imaging (25). However, in future studies, further verification and optimization of the cancer criteria for *in vivo* QME scans may be necessary across a larger patient population. In addition, the quantitative measurement helped to minimize variations among physicians, as indicated by the consistent QME results among the five surgeons in this study.

In conclusion, this study demonstrates that a purpose-built handheld QME probe has the potential to detect cancer based on its elevated microscale stiffness by *in vivo* imaging of the surgical cavity. The study demonstrates the potential of *in vivo* QME to provide more complete removal of cancer during BCS. The proposed technique and clinical scanning protocol together pave the way for future clinical studies to determine the reduction in reexcision rate that can be achieved using *in vivo* QME.

Authors' Disclosures

S.L. Chin reports personal fees from OncoRes Medical outside the submitted work. W.M. Allen reports personal fees from OncoRes Medical outside the submitted work. J.D. Anstie reports personal fees from OncoRes Medical during the conduct of the study and personal fees from OncoRes Medical outside the submitted work. L. Chin reports personal fees and other support from OncoRes Medical during the conduct of the study. K. Newman reports personal fees from OncoRes Medical outside the submitted work. C. Thomas reports personal fees from OncoRes Medical outside the submitted work. B.F. Kennedy reports grants from the Department of Health, Western Australia, the Australian Research Council, and OncoRes Medical during the conduct of the study and other support from OncoRes Medical: ownership interest (including patents) outside the submitted work; in addition, B.F. Kennedy has a patent for a device and a method for evaluating a mechanical property of a material Intl. Pub. No. WO/2016/119011, Appl. No. PCT/AU2016/212695, Priority date: 30/01/2015 issued to OncoRes Medical. No disclosures were reported by the other authors.

Authors' Contributions

P. Gong: Conceptualization, data curation, software, formal analysis, validation, investigation, visualization, methodology, writing–original draft, writing–review and editing. **S.L. Chin:** Data curation, formal analysis, validation, investigation, writing–review and editing. **W.M. Allen:** Conceptualization, data curation, software, formal analysis, validation, investigation, methodology, project administration, writing–review and editing. **H. Ballal:** Resources, data curation, investigation, project administration, writing–review and editing. **J.D. Anstie:** Investigation, methodology, writing–review and editing. **L. Chin:** Data curation, software, formal analysis, visualization, methodology, writing–review and editing. **H.M. Ismail:** Data curation, investigation, methodology, writing–review and editing. **R. Zilkens:** Data curation, formal analysis, validation, methodology, project administration, writing–review and editing. **D.D. Lakhiani:** Data curation, formal analysis, methodology, writing–review and editing. **M. McCarthy:** Software, methodology, writing–review and editing. **Q. Fang:** Data curation, writing–review and editing. **D. Firth:** Methodology, writing–review and editing. **K. Newman:** Methodology, writing–review and editing. **C. Thomas:** Methodology, writing–review and editing. **J. Li:** Formal analysis, writing–review and editing. **R.W. Sanderson:** Formal analysis, writing–review and editing. **K.Y. Foo:** Data curation, writing–review and editing. **C. Yeomans:** Resources, data curation, formal analysis, writing–review and editing. **B.F. Dessauvagie:** Resources, data curation, formal analysis, writing–review and editing. **B. Latham:** Conceptualization, resources, data curation, formal analysis, writing–review and editing. **C.M. Saunders:** Conceptualization, resources, data curation, formal analysis, supervision, investigation, methodology, writing–review and editing. **B.F. Kennedy:** Conceptualization, resources, data curation, formal analysis, supervision, funding acquisition, investigation, methodology, writing–review and editing.

Acknowledgments

The authors gratefully acknowledge Dr. Jose Cid Fernandez, Dr. Saud Hamza, and Nancy Mathew for assistance with clinical scanning and Brett Stone for assistance with sterilization at Fiona Stanley Hospital.

The publication costs of this article were defrayed in part by the payment of publication fees. Therefore, and solely to indicate this fact, this article is hereby marked "advertisement" in accordance with 18 USC section 1734.

Note

Supplementary data for this article are available at Cancer Research Online (http://cancerres.aacrjournals.org/).

Received February 17, 2022; revised May 29, 2022; accepted September 8, 2022; published first September 13, 2022.

References

1. Breast cancer facts and figures 2019–2020. Atlanta, GA: American Cancer Society; 2019.
2. Hershman DL, Buono D, Jacobson JS, McBride RB, Tsai WY, Joseph KA, et al. Surgeon characteristics and use of breast conservation surgery in women with early stage breast cancer. Ann Surg 2009;249:828–33.
3. Katipamula R, Degnim AC, Hoskin T, Boughey JC, Loprinzi C, Grant CS, et al. Trends in mastectomy rates at the Mayo Clinic Rochester: effect of surgical year and preoperative magnetic resonance imaging. J Clin Oncol 2009;27:4082–8.
4. McCahill LE, Single RM, Bowles EJA, Feigelson HS, James TA, Barney T, et al. Variability in reexcision following breast conservation surgery. JAMA 2012;307:467–75.
5. Landercasper J, Whitacre E, Degnim AC, Al-Hamadani M. Reasons for re-excision after lumpectomy for breast cancer: insight from the American Society of Breast Surgeons Mastery (SM) database. Ann Surg Oncol 2014;21:3185–91.
6. Kaczmarski K, Wang P, Gilmore R, Overton HN, Euhus DM, Jacobs LK, et al. Surgeon re-excision rates after breast-conserving surgery: a measure of low-value care. J Am Coll Surg 2019;228:504–12.
7. Waljee JF, Hu ES, Newman LA, Alderman AK. Predictors of re-excision among women undergoing breast-conserving surgery for cancer. Ann Surg Oncol 2008;15:1297–303.
8. Fisher S, Yasui Y, Dabbs K, Winget M. Re-excision and survival following breast conserving surgery in early stage breast cancer patients: a population-based study. BMC Health Serv Res 2018;18:94.
9. Menes TS, Tartter PI, Bleiweiss I, Godbold JH, Estabrook A, Smith SR. The consequence of multiple re-excisions to obtain clear lumpectomy margins in breast cancer patients. Ann Surg Oncol 2005;12:881–5.
10. Pradipta AR, Tanei T, Morimoto K, Shimazu K, Noguchi S, Tanaka K. Emerging technologies for real-time intraoperative margin assessment in future breast-conserving surgery. Adv Sci 2020;7:1901519.
11. Esbona K, Li Z, Wilke LG. Intraoperative imprint cytology and frozen section pathology for margin assessment in breast conservation surgery: a systematic review. Ann Surg Oncol 2012;19:3236–45.
12. Olson TP, Harter J, Muñoz A, Mahvi DM, Breslin T. Frozen section analysis for intraoperative margin assessment during breast-conserving surgery results in low rates of re-excision and local recurrence. Ann Surg Oncol 2007;14:2953–60.
13. St John ER, Al-Khudairi R, Ashrafian H, Athanasiou T, Takats Z, Hadjiminas DJ, et al. Diagnostic accuracy of intraoperative techniques for margin assessment in breast cancer surgery: a meta-analysis. Ann Surg 2017;265:300–10.
14. Heidkamp J, Scholte M, Rosman C, Manohar S, Fütterer JJ, Rovers MM. Novel imaging techniques for intraoperative margin assessment in surgical oncology: a systematic review. Int J Cancer 2021;149:635–45.
15. Butler-Henderson K, Lee AH, Price RI, Waring K. Intraoperative assessment of margins in breast conserving therapy: a systematic review. Breast 2014;23:112–9.
16. Thill M, Baumann K, Barinoff J. Intraoperative assessment of margins in breast conservative surgery: still in use? J Surg Oncol 2014;110:15–20.
17. McCormick JT, Keleher AJ, Tikhomirov VB, Budway RJ, Caushaj PF. Analysis of the use of specimen mammography in breast conservation therapy. Am J Surg 2004;188:433–6.
18. Dupont E, Tsangaris T, Garcia-Cantu C, Howard-McNatt M, Chiba A, Berger AC, et al. Resection of cavity shave margins in stage 0-III breast cancer patients undergoing breast conserving surgery: a prospective multi-center randomized controlled trial. Ann Surg 2021;273:876–81.
19. Chen K, Zhu L, Chen L, Li Q, Li S, Qiu N, et al. Circumferential shaving of the cavity in breast-conserving surgery: a randomized controlled trial. Ann Surg Oncol 2019;26:4256–63.
20. Kennedy KM, Chin L, McLaughlin RA, Latham B, Saunders CM, Sampson DD, et al. Quantitative micro-elastography: imaging of tissue elasticity using compression optical coherence elastography. Sci Rep 2015;5:15538.
21. Huang D, Swanson EA, Lin CP, Schuman JS, Stinson WG, Chang W, et al. Optical coherence tomography. Science 1991;254:1178–81.
22. Drexler W, Fujimoto JG. Optical coherence tomography: technology and applications. Cham: Springer International Publishing AG; 2015.
23. Kennedy BF, McLaughlin RA, Kennedy KM, Chin L, Wijesinghe P, Curatolo A, et al. Investigation of optical coherence microelastography as a method to visualize cancers in human breast tissue. Cancer Res 2015;75:3236–45.
24. Zhou C, Cohen DW, Wang Y, Lee HC, Mondelblatt AE, Tsai TH, et al. Integrated optical coherence tomography and microscopy for ex vivo multiscale evaluation of human breast tissues. Cancer Res 2010;70:10071–9.
25. Kennedy KM, Zilkens R, Allen WM, Foo KY, Fang Q, Chin L, et al. Diagnostic accuracy of quantitative micro-elastography for margin assessment in breast-conserving surgery. Cancer Res 2020;80:1773–83.
26. Kennedy BF, Wijesinghe P, Sampson DD. The emergence of optical elastography in biomedicine. Nat Photon 2017;11:215–21.
27. Gubarkova EV, Sovetsky AA, Zaitsev VY, Matveyev AL, Vorontsov DA, Sirotkina MA, et al. OCT-elastography-based optical biopsy for breast cancer delineation and express assessment of morphological/molecular subtypes. Biomed Opt Express 2019;10:2244–63.
28. Allen WM, Kennedy KM, Fang Q, Chin L, Curatolo A, Watts L, et al. Wide-field quantitative micro-elastography of human breast tissue. Biomed Opt Express 2018;9:1082–96.
29. Allen WM, Chin L, Wijesinghe P, Kirk RW, Latham B, Sampson DD, et al. Wide-field optical coherence micro-elastography for intraoperative assessment of human breast cancer margins. Biomed Opt Express 2016;7:4139–53.
30. Povoski SP, Jimenez RE, Wang WP, Xu RX. Standardized and reproducible methodology for the comprehensive and systematic assessment of surgical resection margins during breast-conserving surgery for invasive breast cancer. BMC Cancer 2009;9:254.
31. Héquet D, Bricou A, Koual M, Ziol M, Feron JG, Rouzier R, et al. Systematic cavity shaving: modifications of breast cancer management and long-term local recurrence, a multicentre study. Eur J Surg Oncol 2013;39:899–905.
32. Mansilla-Polo M, Ruiz-Merino G, Marín-Rodríguez P, Iborra-Lacal E, Guzmán-Aroca F, de Lema CMSP, et al. Cavity shaving for invasive breast cancer conservative surgery: reduced specimen volume and margin positive rates. Surg Oncol 2021;38:101632.
33. Allen WM, Foo KY, Zilkens R, Kennedy KM, Fang Q, Chin L, et al. Clinical feasibility of optical coherence micro-elastography for imaging tumor margins in breast-conserving surgery. Biomed Opt Express 2018;9:6331–49.
34. Tadros AB, Smith BD, Shen Y, Lin H, Krishnamurthy S, Lucci A, et al. Ductal carcinoma in situ and margins <2 mm: contemporary outcomes with breast conservation. Ann Surg 2019;269:150–7.
35. Moran MS, Schnitt SJ, Giuliano AE, Harris JR, Khan SA, Horton J, et al. Society of Surgical Oncology-American Society for Radiation Oncology consensus guideline on margins for breast-conserving surgery with whole-breast irradiation in stages I and II invasive breast cancer. Ann Surg Oncol 2014;21:704–16.
36. Morrow M, Van Zee KJ, Solin LJ, Houssami N, Chavez-MacGregor M, Harris JR, et al. Society of Surgical Oncology-American Society for Radiation Oncology-American Society of Clinical Oncology consensus guideline on margins for breast-conserving surgery with whole-breast irradiation in ductal carcinoma in situ. Ann Surg Oncol 2016;23:3801–10.
37. Langhans L, Tvedskov TF, Klausen TL, Jensen MB, Talman ML, Vejborg I, et al. Radioactive seed localization or wire-guided localization of nonpalpable invasive and in situ breast cancer: a randomized, multicenter, open-label trial. Ann Surg 2017;266:29–35.
38. de Boniface J, Szulkin R, Johansson ALV. Survival after breast conservation vs mastectomy adjusted for comorbidity and socioeconomic status: a Swedish national 6-year follow-up of 48 986 women. JAMA Surg 2021;156:628–37.
39. Kim KJ, Huh SJ, Yang JH, Park W, Nam SJ, Kim JH, et al. Treatment results and prognostic factors of early breast cancer treated with a breast conserving operation and radiotherapy. Jpn J Clin Oncol 2005;35:126–33.
40. Atkins J, Al Mushawah F, Appleton CM, Cyr AE, Gillanders WE, Aft RL, et al. Positive margin rates following breast-conserving surgery for stage I-III breast cancer: palpable versus nonpalpable tumors. J Surg Res 2012;177:109–15.
41. Garra BS, Cespedes EI, Ophir J, Spratt SR, Zuurbier RA, Magnant CM, et al. Elastography of breast lesions: initial clinical results. Radiology 1997;202:79–86.
42. McKnight AL, Kugel JL, Rossman PJ, Manduca A, Hartmann LC, Ehman RL. MR elastography of breast cancer: preliminary results. Am J Roentgenol 2002;178:1411–7.
43. Levental KR, Yu H, Kass L, Lakins JN, Egeblad M, Erler JT, et al. Matrix crosslinking forces tumor progression by enhancing integrin signaling. Cell 2009;139:891–906.

44. Butcher DT, Alliston T, Weaver VM. A tense situation: forcing tumour progression. Nat Rev Cancer 2009;9:108–22.
45. Acerbi I, Cassereau L, Dean I, Shi Q, Au A, Park C, et al. Human breast cancer invasion and aggression correlates with ECM stiffening and immune cell infiltration. Integr Biol 2015;7:1120–34.
46. Dvorak HF, Weaver VM, Tlsty TD, Bergers G. Tumor microenvironment and progression. J Surg Oncol 2011;103:468–74.
47. Zaha DC. Significance of immunohistochemistry in breast cancer. World J Clin Oncol 2014;5:382–92.
48. Lee H, Akers W, Bhushan K, Bloch S, Sudlow G, Tang R, et al. Near-infrared pH-activatable fluorescent probes for imaging primary and metastatic breast tumors. Bioconjugate Chem 2011;22:777–84.
49. Tanei T, Pradipta AR, Morimoto K, Fujii M, Arata M, Ito A, et al. Cascade reaction in human live tissue allows clinically applicable diagnosis of breast cancer morphology. Adv Sci 2019;6:1801479.
50. Ueo H, Shinden Y, Tobo T, Gamachi A, Udo M, Komatsu H, et al. Rapid intraoperative visualization of breast lesions with γ-glutamyl hydroxymethyl rhodamine green. Sci Rep 2015;5:12080.